Dalton Transactions

Accepted Manuscript

This article can be cited before page numbers have been issued, to do this please use: X. Ma, Y. Liu, W. Song, Z. Wang, X. Liu, G. Xie, S. Chen and S. Gao, *Dalton Trans.*, 2018, DOI: 10.1039/C8DT02335B.

This is an Accepted Manuscript, which has been through the Royal Society of Chemistry peer review process and has been accepted for publication.

Accepted Manuscripts are published online shortly after acceptance, before technical editing, formatting and proof reading. Using this free service, authors can make their results available to the community, in citable form, before we publish the edited article. We will replace this Accepted Manuscript with the edited and formatted Advance Article as soon as it is available.

You can find more information about Accepted Manuscripts in the author guidelines.

Please note that technical editing may introduce minor changes to the text and/or graphics, which may alter content. The journal's standard Terms & Conditions and the ethical guidelines, outlined in our author and reviewer resource centre, still apply. In no event shall the Royal Society of Chemistry be held responsible for any errors or omissions in this Accepted Manuscript or any consequences arising from the use of any information it contains.

ROYAL SOCIETY OF CHEMISTRY

rsc.li/dalton

View Article Online
DOI: 10.1039/C8DT02335B

Journal Name

ARTICLE

A Difunctional Azido-Cobalt(II) Coordination Polymer Exhibiting Slow Magnetic Relaxation Behaviour and High-Energy Characteristics with Good Thermostability and Insensitivity

Received 00th January 20xx,
Accepted 00th January 20xx

DOI: 10.1039/x0xx00000x

www.rsc.org/

Xiaohui Ma,[a] Yaru Liu,*[b] Weiming Song,[a] Zheng Wang,[a] Xiangyu Liu,*[a] Gang Xie,[c] Sanping Chen*[c] and Shengli Gao[c]

A novel one-dimensional azido-cobalt(II) compound, $[Co_2(1\text{-mbt})_2(N_3)_4]_n$ (**1**) (1-mbt = 1-((2-propyl-imidazol-1-yl)methyl)-benzo[1,2,3]triazole), has been solvothermally synthesized. X-ray crystal structure analysis demonstrates that two crystallographically independent Co(II) atoms in the asymmetrical unit of compound **1** exhibit rectangular pyramid geometry. The 3D supermolecular network of **1** consists of well-isolated 1D metal chains in which the azido bridging ligands assume an unusual pattern of combination with the Co(II) centre as the sign of $[\text{-EE-EO-EO-EO-}]_n$. The various coordination modes of the azido anion are responsible for different magnetic exchanges between the adjacent Co(II) ions. The end-to-end (EE) mode mediates the antiferromagnetic coupling, whereas the end-on (EO) manner contributes to the ferromagnetic interaction. Magneto-structure relationships are discussed with the aid of theoretical calculations which are employed to find the potential single-ion magnetic anisotropy and reproduce properly the observed magnetic coupling. Alternating current magnetic susceptibility measurements reveal that **1** features a typical behaviour of field-induced slow magnetic relaxation. Energetic characterizations evidence that the resulting compound possesses satisfactory detonation properties, superior lack of sensitivity and thermostability owing to the high nitrogen content (N% = 40.10%) and coherent intrachain configuration. The kinetic parameters of the exothermic processes for **1** are investigated by the Kissinger method and the Ozawa method. We note that **1** has potential application prospects as a new generation of environmentally friendly high-energy materials based on this nitrogen-rich and oxygen-free system. In addition, the compound is developed as a practical additive to promote the thermal decomposition of ammonium perchlorate (AP) and hexahydro-1,3,5-trinitro-1,3,5-triazine (RDX). The finding in this work highlights an example of effective development of advanced magneto-energetic materials.

Introduction

Coordination polymers (CPs) yielded by metal ions and organic ligands have attracted considerable attention in the fields of coordination chemistry and materials science for their wide application in sensors,[1] gas storage,[2] magnetic materials[3] and high-energy materials.[4] Usually, the main physical features of CPs are attributed to the nature of the metal centre as well as to the properties of the ligands. Nonetheless, it is difficult to satisfy the requirements of the assembly process to obtain the desired behavioural and structural motifs. The exploration of such molecular materials that exhibit dramatic property, or even multifunctionalities is a significant and challenging theme in materials science.

It is well known that CPs in which paramagnetic metal ions are bridged by short ligands have evoked much interest not only for understanding the fundamental relationship between structure and magnetism but also for constructing new magnetic materials with potential applications[5] in information storage,[6] quantum computing,[7] and spintronics.[8] In this sense, the Co(II) ion as paramagnetic metal ion with strong spin-orbit coupling, has been widely adopted to construct the expected coordination polymers, which may exhibit dramatic magnetic behaviours due to the flexible zero-field splitting parameter and large magnetic anisotropy of the Co(II) centre.[9] As a short ligand, the azide anion (N^{3-}) with linear shape and delocalization of its π-electrons on the three nitrogen atoms can effectively propagate the magnetic interaction between the paramagnetic centres, giving rise to the formation of numerous coordination compounds with fascinating architectures and magnetic properties. It has been reported

[a] *State Key Laboratory of High-efficiency Utilization of Coal and Green Chemical Engineering, College of Chemistry and Chemical Engineering, Ningxia University, Yinchuan 750021, China. E-mail: xiangyuliu432@126.com; Tel.: +86-951-2062004; Fax: +86-951-2062860*

[b] *School of Science, North University of China, Taiyuan 030051, China. E-mail: liuyr326@163.com*

[c] *Key Laboratory of Synthetic and Natural Functional Molecule Chemistry of Ministry of Education, College of Chemistry and Materials Science, Northwest University, Xi'an 710069, China. E-mail: sanpingchen@126.com*

Electronic Supplementary Information (ESI) available: Figs. S1-S5, Tables S1-S8, crystal structure of compound **1** in CIF format CCDC number is 1821186 (**1**). These data can be obtained free of charge from the Cambridge Crystallographic Data Centre via www.ccdc.cam.ac.uk/data_request/cif.

View Article Online
DOI: 10.1039/C8DT02335B

that N^{3-} is able to bridge metal centres in the end-on (EO) mode, end-to-end (EE) mode, or other modes, leading to a number of low-dimensional materials with abundant structural variety (see Scheme 1) and a series of diverse magnetic interactions.[10] Up to now, different combinations of EO and EE modes have resulted in a handful of alternating azdio-Co(II) chains with $[\text{-EO-EE-}]_n$, $[\text{-EO-EO-EE-}]_n$, and $[\text{-EO-EE-EE-}]_n$ sequences showing interesting magnetic properties.[10d-g] It is well-determined that the end-to-end mode generally transmits the antiferromagnetic (AF) coupling while the end-on mode encourages the ferromagnetic (F) coupling. A high number of azido-bridged discrete polynuclear and infinite polymeric systems with different dimensionality and magnetic properties have been demonstrated,[11] including some long range ordered materials and a few molecule-based magnets.[12] In these materials, spin carriers with large magnetic anisotropy (preferably of the Ising type) and azido bridging ligands favouring strong intrachain magnetic coupling (*J*) are the essential ingredients for molecular magnetic materials.

Furthermore, as noticed, the azido ligand has attracted intense attention and is the simplest nitrogen-rich ligand with the highest nitrogen content of 100%, which is a prominent energetic moiety that can increase the heat of formation to approximately 355 kJ mol^{-1}; additionally, the azido combustion products are environmentally friendly [13] Compared to the preparations of poisonous and polluting primary explosives such as lead azide, lead styphnate (2,4,6-trinitroresorcinate) or mercury fulminate, an alternative approach to obtain new-generation green energetic materials with excellent properties is to use environmentally friendly energetic ligands to bridge non-toxic metal ions using coordination chemistry methods. However, because of the extreme sensitivity of azido, the reports of exploration of the high-energy performance of azido derivatives, let alone azido-metal coordination polymers, have been rather limited. Although a previous study has proven that the sensitivity of the azide compound depends on the minimum distance between the N atoms of adjacent azides,[14] how to fine-tune the structures to achieve the desired balance of the energy and sensitivity of azido-based compounds has been a topic of interest and still poses a difficulty in the field of energetic materials. To improve the insensitivity and the stability of such highly explosive compositions, the introduction of insensitive co-ligands with good mechanical strengths and rigid frameworks into existing transition-metal azido systems has been identified as a feasible approach to create more complex structures and thus achieve a compromise in the conflict between high energy and safety for target materials.

Inspired by the above background, in this work, a new azido-Co(II) coordination polymer, $[Co_2(1\text{-mbt})_2(N_3)_4]_n$ (**1**), was obtained with a stable N-heterocycle component (1-mbt) as coligand. The crystal structure, magnetic and energetic properties of the as-prepared compound have been investigated. Notably, a novel bridging sequence of azido fragment $[\text{-EE-EO-EO-EO-}]_n$ bonds with metal centres is obtained to yield a 1D cobalt chain and transmit diverse magnetic couplings between the adjacent Co(II) ions. To the best of our knowledge, azido-Co(II) architecture with $[\text{-EO-EO-EO-EE-}]_n$ sequence has not yet been reported. The intrachain magnetic interactions are further confirmed by DFT calculations. The measurement results illustrate that **1** performs an inspiring field-induced slow relaxation of magnetization. The magneto-structural correlations are also discussed. Moreover, the thermal stability, non-isothermal kinetics analysis, sensitivity, standard molar enthalpy of formation and the corresponding detonation properties of **1** are explored in detail. The catalytic effects of **1** towards the thermal decompositions of AP and RDX are examined as well. The present candidate material is anticipated to be one of the preeminent multifunctional materials for use in magneto-energetic fields.

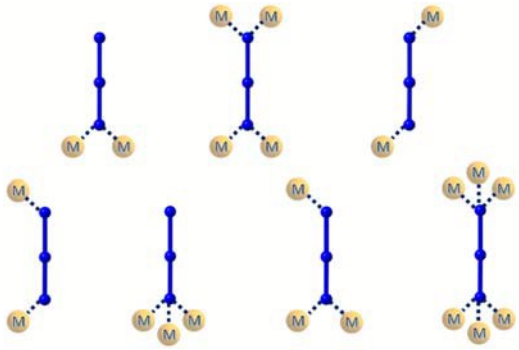

Scheme 1 Coordination modes of bridging azido

Results and discussion

Crystal structure

Single-crystal X-ray structure analyses determined that compound **1** was crystallized in the triclinic space group *P*-1. There are two crystallographically independent Co(II) atoms in the asymmetrical unit of compound **1**. Co1 assumes a rectangular pyramid completed by the two nitrogen atoms (N3 and N4) from the two EO azido ions (Co1-N3 = 2.021(3) Å, Co1-N4 = 1.994(3) Å), two nitrogen atoms (N7 and N5A) from the two end-to-end (EE) azido ions (Co1-N7 = 2.408(4) Å, Co1-N5A = 1.978(4) Å), an another nitrogen atom (Co1-N1 =1.978(3) Å) from the imidazole of 1-mbt. The Co2 atom resides on a centre of rectangular pyramid, which is different from that observed in Co1, with four nitrogen atoms (N3, N4, N8, and N8A) from the four EO azido ligands (Co2-N3 = 2.015(3) Å, Co2-N4 = 2.032(3) Å, Co2-N8 = 2.432(3) Å, Co2-N8A = 1.982(3) Å) and one nitrogen atom (Co2-N2 = 1.974(3) Å) from the imidazole (Fig. 1a). As found in **1**, the Co1 and Co2 atoms are doubly linked by two EO azido bridges with similar bridging angles (Co1-N-Co2 = 100.26°). The nearby Co2 atoms are also doubly joined by two EO azido ions with similar bridging angles (Co2-N-Co2 = 94.76°). Through such bridges, the neighbouring two Co2 are linked to one Co1 atom to form a linear tetranuclear motif. Neighbouring Co1 atoms from different tetranuclear units are doubly linked by two EE azido groups, and hence an infinite chain is formed (Fig. 1b). The distances spanned by the

View Article Online
DOI: 10.1039/C8DT02335B

double EO azido ligands are 3.09 Å (Co1···Co2) and 3.26 Å (Co2···Co2), while the Co1…Co1 distances crossed by the twofold EE azido groups are much longer (5.12 Å), implying three different exchange couplings between Co(II) ions in the compound (Fig. 1). As is found for most compounds with double EE-azido bridges, compound **1** assumes chair conformation with the two linkers being coplanar. All Co(II) chains have been constructed in the supramolecular framework of **1** (Fig. S1). The shortest distance between the interchain Co(II) ions is 11.28 Å.

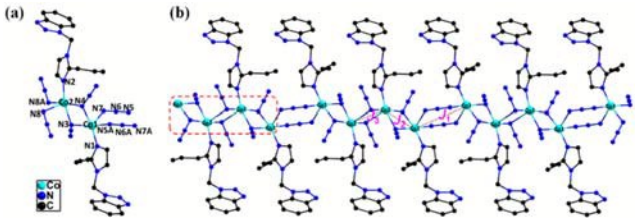

Fig. 1 (a) Coordination environment of the Co(II) centre in **1**. (Hydrogen atoms are omitted for clarity) (b) The 1D chain with mixed EO and EE azido bridges for **1**. (Hydrogen atoms are omitted for clarity).

Magnetic studies

Static magnetic properties On the basis of the dinuclear Co(II) units coupled by EO-azido and EE-azido bridges, magnetic measurements were carried out on polycrystalline samples of compound **1**, and the phase purity of the bulk materials was confirmed by PXRD (Fig. S2). The temperature dependence of the magnetic susceptibility was investigated in the temperature range of 2-300K (Fig. 2). At 300 K, the $\chi_M T$ value of **1** is 2.81 $cm^3\ mol^{-1}\ K$ which is clearly larger than the spin-only value of 1.875 $cm^3\ mol^{-1}\ K$ for a high-spin Co(II) ion (S = 3/2 and g = 2), indicating the presence of a significant orbital contribution to the magnetic moment. Upon cooling, the $\chi_M T$ curve for **1** decreases slowly to 100 K, even though a barely visible increase from 300 K to 200 K is perceived and can be due to experimental errors. Subsequently, the $\chi_M T$ product decreases sharply below 100 K to the minimums of 1.71 $cm^3\ mol^{-1}\ K$ at 2 K. Fitting of the magnetic data in the temperature range of 2–300 K using the Curie–Weiss law gives the Curie constant C = 2.87 $cm^3\ mol^{-1}\ K$ and the Weiss temperature ϑ = -2.35 K (Fig. S3). The negative ϑ value of the Weiss constant and the initial decrease of $\chi_M T$ could be a result of the occurrence of significant spin-orbit coupling or antiferromagnetic interaction between the high-spin Co(II) ions. Considering the complexity of the structure of **1**, quantitative analyses on the magnetic data for the exchange magnetic interactions and magnetic anisotropies are inherently difficult. Many different parameters must be considered to model these magnetic data. For **1,** there are three nearest exchange interactions between the Co(II) cations (namely, J_1, J_2, J_3), with the spin Hamiltonian

$$H = -\sum_{i=0}^{\infty}[J_1 S_{4i+1}S_{4i+2} + J_2 S_{4i+2}S_{4i+3} + J_3 S_{4i+3}S_{4i+4} + J_2 S_{4i+4}S_{4i+5}]$$

Meanwhile, the significant contribution of the orbital momentum in Co(II) ion should be concerned in view of the decrease of the $\chi_M T$ data with decreasing temperature. Take account of the above Hamiltonian and the spin–orbit coupling parameter λ etc., the experimental data were fitted by using the MAGPACK software package[15] yielding J_1 (Co1-Co1) = -18.36 cm^{-1}, J_2 (Co1-Co2) = 20.87 cm^{-1}, J_3 (Co2-Co2) = 2.04 cm^{-1}, g = 2.6, λ = -104 cm^{-1}, α =1.28 and Δ = 387 cm^{-1} with R = 2.9 × 10^{-5} [$R = \sum(\chi_{obs}-\chi_{calc})^2/\sum(\chi_{obs})^2$]. Considering the approximation of the model, these parameters should be taken as a rough estimation. Nevertheless, the best fitting result of the negative value of J_1 suggests the existence of the antiferromagnetic (AF) coupling, while positive values of J_2 and J_3 support the ferromagnetic (F) coupling. As previously reported in the literature, azido bridges in the end-end (EE) mode usually mediate the AF coupling, whereas the end-on (EO) mode results in the F interactions.[16]

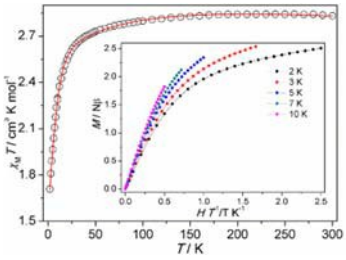

Fig. 2 $\chi_M T$ *vs.* T plots for **1**, the solid line is the fit to the experimental data. Inset: Experimental M versus HT^{-1} plots of **1** at different temperatures.

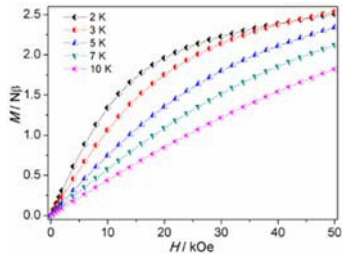

Fig. 3 Magnetization *vs*. H plots for **1** at different temperatures.

As shown in Fig. 3, the M versus H curves (where M is the magnetization per Co(II) unit and H is the applied dc magnetic field) were determined in the range from the zero DC field to 5 T at 2, 3, 5, 7, and 10 K for **1**. The highest values of 2.53 Nβ is reached for **1** at 5 T and is well below the theoretical saturation limit for an S = 3/2 system (M_{sat} = 3.3 with g = 2). The magnetization value does not saturate even at the highest available field, with one accord of the magnetic anisotropy. Moreover, the field-dependent magnetisations in the form of the M *vs.* HT^{-1} plots for **1** were obtained (Fig. 2 inset). For **1**, the M *vs.* HT^{-1} plots at different temperatures are not superimposed, further strengthening the presence of

View Article Online
DOI: 10.1039/C8DT02335B

significant magnetic anisotropy, which is attributed to the strong spin-orbital coupling of the Co(II) ion.

Dynamic magnetic properties To examine the spin dynamics, alternating-current (ac) magnetic susceptibility studies for compound **1** were conducted under a zero dc field with the frequency of 1000 Hz and the temperature range of 2-15 K. No out-of-phase (χ_M″) signal can be observed for **1** until the temperature drops to 2 K (Fig. S4), implying a fast quantum tunnelling of the magnetization (QTM) through the spin-reversal barrier. To find a suitable applied magnetic field that can suppress the QTM effect, the dependence of the χ_M″ signal of **1** on the applied dc field strength at 2 K and 1000 Hz was measured. A χ_M″ signal with a significant sharp peak at approximately 2000 Oe dc field supposes field-induced slow magnetic relaxation operating in **1**. Under this optimal dc field, the ac susceptibility measurements were applied in the 2-8 K range and at frequencies of 1, 33, 100, 333, 500, 800 and 1000 Hz for **1** (Fig. 4). Both χ_M′ and χ_M″ susceptibilities in **1** feature weak temperature dependence in the relatively low temperature region, which is a signature of a slow magnetic relaxation, and it is found that the probable relaxation behaviour through the QTM process is substantially depressed under a static field of 2000 Oe. At the selected frequencies, **1** goes through a maximum shifting to high temperature with increasing frequency, which is the sign of a superparamagnet. In addition, the change of the peak temperatures (T_p) in the χ_M″ plots determined by the Mydosh parameter $\phi = (\Delta T_p/T_p)/(\Delta \log f)$ is estimated to be 0.23 which falls in the normal range ($0.1 < \phi < 0.3$) expected for superparamagnetic behaviour.

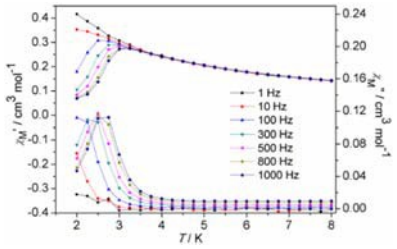

Fig. 4 Temperature dependence of the in-phase and out-of phase ac susceptibility signals under 2000 Oe dc field of **1** at frequencies in the range 1-1000 Hz.

To further explore the dynamics of the magnetization of **1**, the frequency-dependent ac magnetic data experiments were characterized for **1** at temperatures ranging from 2 to 4 K (Fig. 5). The χ_M′ and χ_M″ signals of **1** show frequency dependences. Obviously, the slow relaxation of the magnetization in **1** can be detected. Additionally, the peaks of χ_M″ in **1** do not rise sharply at the low-temperature and low-frequency regime, suggesting that the applied field of 2000 Oe is appropriate for suppressing the QTM effects. The magnetization relaxation time (τ) is derived from the frequency-dependent measurements and is plotted as a function of $1/T$ in Fig. 6. The τ of compound **1** acts as linear extrapolations (thermally activated regimes) at high temperatures and is well-described by the Arrhenius law, $\tau = \tau_0 \exp(U_{eff}/k_BT)$, characteristic of a thermally activated mechanism involving a barrier U_{eff} for the reversal of magnetization. A fit to the linear relationship extracts the effective energy barrier U_{eff} = 22.46 K (16.25 cm^{-1}) with τ_0 = 3.31× 10^{-8} s, which is consistent with the expected τ_0 of 10^{-6}-10^{-11} for a super-paramagnet. As reported in the earlier studies, the effective energy barrier of a polynuclear cobalt(II) cluster can be attributed to two components, namely, the energy barrier for the magnetic anisotropy of the individual metal ions and the correlation energy originating from the intermetallic magnetic coupling. Although it is not possible to experimentally extract any meaningful parameters for the magnetic anisotropies in view of their complicated chain structures and existence of two different Co(II) centres,[17] the field-induced slow relaxation of the magnetization in **1** could be resulted from the 1D pattern—the Ising-type chain combining the strong anisotropy from the orbitally degenerate Co(II) nodes and the ferromagnetic coupling through the EO-azido bridges. An important note about this work is that the present case with 1D chain-like topology is operative of a characteristic superparamagnetic behaviour under an applied dc field, rather than so called single-chain magnet which usually exhibits zero-field slow relaxation of magnetization.

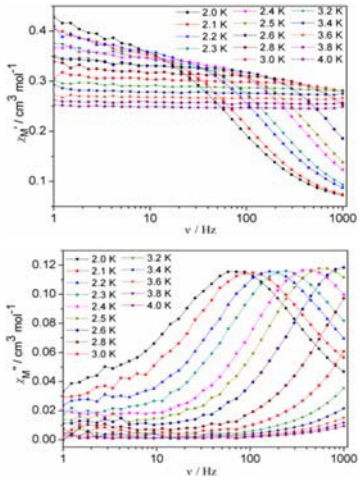

Fig. 5 Frequency dependence of the in-phase (top) and out-of phase (bottom) ac susceptibility signals for **1** under 2000 Oe dc field.

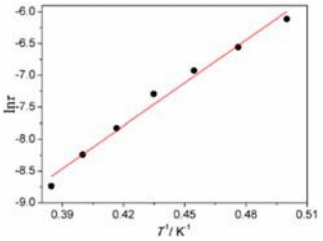

Fig. 6 Temperature dependence of the magnetization relaxation rates of **1**. The solid red line was fitted using the Arrhenius equation.

View Article Online
DOI: 10.1039/C8DT02335B

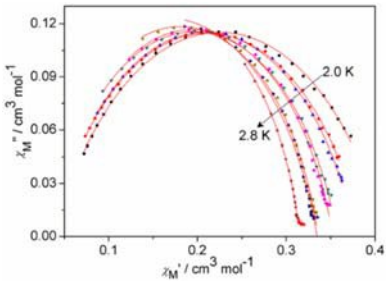

Fig. 7 The Cole–Cole plots at 2.0–2.8 K of **1** under 2000 Oe.

Cole–Cole plots of χ_M'' *vs.* χ_M' (Fig. 7) from 2 to 2.8 K for **1** display an ideal semi-circular shape, and are generated from the frequency-dependent ac susceptibility data. The semi-circular plots can be fitted by using the generalized Debye model. This fitting provides a value for the parameter α, which is related to the width of the distribution of the relaxation times; that is, α = 1 corresponds to an infinitely wide distribution of the relaxation times, whereas α = 0 describes a single relaxation process. The values of the parameter α (Table S1) is in the range of 0.12-0.29, suggesting a narrow distribution of relaxation times and is in agreement with the existence of a single relaxation process in that temperature region.

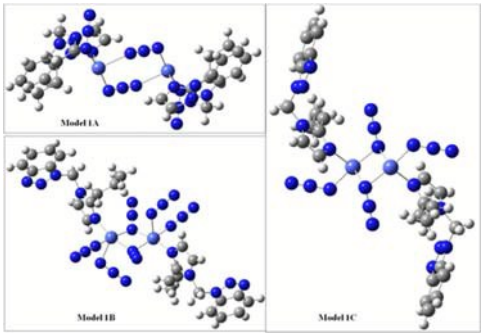

Fig. 8 Magnetic cores used for computational studies (Co1-J_1-Co1 of Model 1A, Co1-J_2-Co2 of Model 1B, Co2-J_3-Co2 of Model 1C).

Theoretical study To further elucidate the ferromagnetic nature of the exchange interaction in compound **1**, we performed a theoretical study of the isotropic coupling constants *J* between the Co(II) ions based on DFT calculations at the BP86 and B3LYP level of theory carried out using the ORCA program. According to the structure of **1,** the dominant magnetic exchange is mediated between the adjacent two Co(II) ions through the azido. The calculations for the compound were carried out with the model (for comparison) applied to the magnetic fitting by filling-in all the coordination sites of the Co(II) ions (Fig. 8).

The results of the theoretical calculation and the experimental fitting in terms of the coupling constants are listed in Table S2. The calculated *J* values extracted from all three different equations (see Experimental section) match the experimentally fitted data, further pointing out that the F and AF couplings coexist in compound **1**. Although the calculated values deviate slightly from the fitted values, in all the cases the sign and the relative magnitudes of the exchange parameters are similar to the experimental results. Obviously, the choices of the calculated formulas and the basis sets for these calculations are uniformly suitable for investigation on the title compound. It is difficult to say in general which formula or basis set works better, but it is clear that the results of the theoretical calculation qualitatively and quantitatively verify the measured data; therefore, the tiny differences may result from the fact that the real compound is not a simple entity of the model calculations but rather is has a very complicated overall structure.

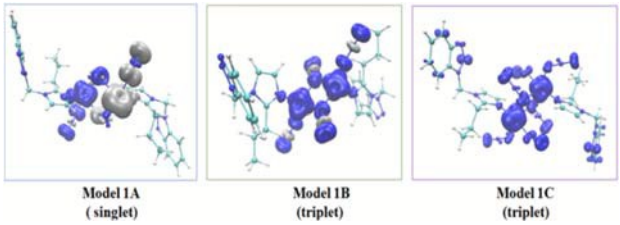

Fig. 9 Spin density maps of the ground spin states calculated for model complexes 1A, 1B and 1C at B3LYP level(for def2-tzvp basis set). Positive and negative spin populations are represented as blue and gray surfaces. The isodensity surfaces correspond to a value of 0.005 e/A^3.

The representation of the spin distribution corresponding to the ground spin states for compound **1** are plotted in Fig. 9. For model 1A, the singlet state is found to be the ground state (which implies the negative exchange parameter, J_1), while for model 1B and 1C, the high-spin triplet states are the ground spin-states (implying positive exchange parameters, J_2 and J_3). The spin density distributions for the triplet ground states for the models 1B and 1C manifest the predominance of the delocalization mechanism. The spin-density analysis reveals that the positive spin densities are very concentrated at the Co(II) ions and the two terminal nitrogen atoms (one of these is the bridging N atom) of the EO-azido groups. This spin density is the origin of the strong ferromagnetic coupling. The rather high spin-densities on the EO-azido bridges in 1B model provide evidence for the moderately strong positive exchange observed experimentally, where the low spin-densities on the EO-azido bridges in the 1C model confirm the weak positive exchange surveyed experimentally (because the magnitude of the exchange is very low). Meanwhile, for model 1A, the same positive and negative spin densities mainly concentrated at the Co(II) ions track the experimentally fitted values, indicating the existence of a moderately strong negative exchange.

In order to obtain an insight of the single-ion magnetic anisotropy for **1**, *ab initio* calculations have been performed as well. It is known that these calculations are costly in terms of computational time, and thus, at this level of theory only molecular fragments with one Co(II) metal center can be

View Article Online
DOI: 10.1039/C8DT02335B

investigated. In accordance with our above-mentioned results, the model structure for the calculation of the single-ion anisotropies of 1 is based on mononuclear Co(II) fragments with sodium ions at the terminating positions. Since the asymmetric unit of compound **1** contains two crystallographically independent Co(II) centres, two simplified model complexes had to be used (Fig. S5). The approach done with ORCA resulted in large negative *D*-values (D = -65.4 cm^{-1} for Co1 and D = -100.6 cm^{-1} for Co2) for compound **1**, respectively. The signs of the calculated *D* constants definitely confirm the easy-axis type of the magnetic anisotropy for **1**. As mentioned above, it is difficult to estimate the accuracy of the theoretical calculation, but the work is only qualitative. This may result from the fact that the real compound is not made up of scattered entities as it has been modelled, but is very complicated across the whole structure. Also, there is large anisotropy of g-tensors from which is obvious that g_x = 1.97, g_y = 2.43, g_z = 2.88 for Co1 and g_x = 1.71, g_y = 2.46, g_z = 3.21 for Co2. The calculated g values (S_{eff} = 3/2) show in accordance with the ZFS an easy-axis anisotropy ($g_z > g_x, g_y$). The large g_z values as compared to penta-coordinated Co(II) cases are the result of a strong spin–orbit contribution. The energy levels and the contributions of the excited spin states to *D*-tensor are listed in Tables S3-S6. It is evident that first excited quartet has a significant contribution to *D* tensor of Co1, while the first three excited quartets are responsible for the *D* factor of Co2.

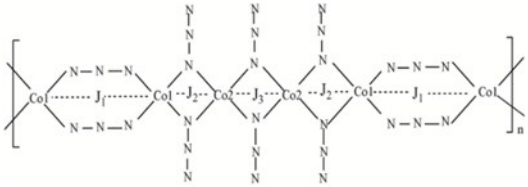

Scheme 2 Schematic representation of the alternation pattern in compound **1**, showing the *J* pathways

Magneto-structural correlation Compound **1** consists of bimetallic structures with each Co(II) centre five-coordinated by four N atoms from different azido anions and one N atom from the 1-mbt ligand, which is more peculiar and has not been reported previously. The azido ligands in the compound display two coordination modes (EO and EE) to connect the adjacent metal ions. In compound **1**, the repeating unit includes four Co(II) ions (Co1-Co2-Co2-Co1) which are linked by two types of EO-azido bridges. These repeating units are combined with the EE-azido linkers to form the novel 1D Co(II) chains which also offer the opportunity to investigate the complicated and fascinating magneto-structural relationships.

As reported in previous studies, 1D metal azido systems present a great variety of structures, and all of these structures are connected with their magnetic behaviours. Thus, we can summarize the different kinds of structures as follows: $[\text{-EE-}]_n$, where all bridges in the end-end (EE) mode usually mediate the antiferromagnetic (AF) coupling; $[\text{-EO-}]_n$, where all bridges in the end-on (EO) mode drive ferromagnetic (F) interactions; $[\text{-EO-EO-EO-EO-EE-}]_n$ with only one EE and some EO bridges behave as canted ferromagnets and antiferromagnets; $[\text{-EO-EE-}]_n$, where double AF and F couplings are observed for ferrimagnets; $[\text{-EO-EE-EE-}]_n$, where the presence of only one EO and some EE groups result in metamagnets. All of these can be interpreted by the correlations between the bridging modes of azido groups and the overall magnetic behaviours. We note that the pattern of $[\text{-EE-EO-EO-EO-}]_n$ in **1** is an unique type of combination with the metal cobalt centre (Scheme 2). The experimental fitting and theoretical calculation have established presence of the AF and F couplings.

As shown in Fig. 10, to fit the experimental results, three exchange coupling parameters (J_1, J_2, J_3) are necessary to compare to those reported for similar systems, J_1 (-18.36 cm^{-1}) with the negative value, is found to be antiferromagnetic, such as in the all EE conformation modes.[18] J_2 (20.87 cm^{-1}) and J_3 (2.04 cm^{-1}) with positive values are ferromagnetic, in agreement with the EO coordination mode. Nevertheless, the value for J_3 is less than that of J_2, and the magnitudes of two parameters from two different dinuclear units with EO-azido indicate an apparent disparity. Considering the structure, a slight difference is perceived between the Co-N-Co angles in the two units (Co1···Co2, Co2···Co2), which are 100.26° and 94.76°, respectively. Even more important, the J_3 is related to a four atoms plane Co2N2 composed by two neighbour Co2 ions and two terminal N atoms of EO-azido bridges with the dihedral angle (Θ) of zero, implying that the EO-azido bridges and the adjacent two Co2 ions are coplanar. However, corresponding to J_2, the plane Co2N2 including nearby Co1 and Co2 ions and two N atoms from the two EO-azido molecules are not coplanar, with a non-zero dihedral angle (Θ = 13.31°). Based on the above discussion, the relatively smaller Co-N-Co angle and the non-coplanarity of the four atoms unit (Co2N2) will enhance the ferromagnetic component.

Besides, the most important contribution to the spin-orbit coupling between the ground and lowest excited states in Co(II) ion stabilizes the largest M_S = 3/2 components of the S = 3/2 state and therefore brings large contribution to *D*. It was calculated that two Co(II) ions in compound **1** possess strong easy-axis magnetic anisotropies expressed by the zero-field-splitting parameters D = -65.4 cm^{-1} and D = -100.6 cm^{-1} for two Co(II) centres, respectively. It is generally accepted that a large positive or negative value of the *D* parameter is a prerequisite of SMM behaviour. Meanwhile, SMM behaviour has also been reported for penta-, hexa-, and hepta-coordinated cobalt(II) complexes with positive or negative *D*.[9] Accordingly, the barrier to spin reversal for this case is moderately governed by the anisotropic parameters *D* that are essential in modifying the easy-axis of magnetization.

Energetic investigations

Thermostability To assess the thermostability of **1**, 0.7 mg crystalline samples of **1** were examined by TG and DSC measurements under the linear heating rate of 10 ˚C·min^{-1} in the nitrogen atmosphere. As depicted in Fig. 10, the DSC curve describes one intense and sharp exothermic process with the peak temperature of 201 °C. As can be seen from the TG curve, a one-step mass-loss stage is detected, corresponding to the

View Article Online
DOI: 10.1039/C8DT02335B

single peak in the DSC curve. A sudden weight loss appears at 190 °C, which stops at 240 °C and is attributed to the full decomposition process for the main framework of the compound. The final products (Co and C) were proved by ICP-AES and elementary analysis, with the residue mass percentage of 55.10% which is in agreement with the calculated value of 55.95%. TG and DSC analyses illustrate a potential explosive performance and the relatively good thermal stability of **1.**

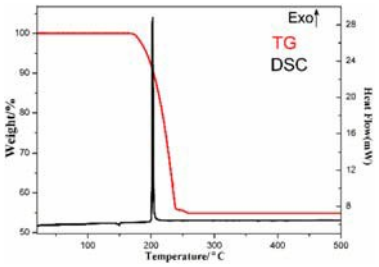

Fig. 10 TG-DSC curves of **1** at heating rate of 10 °C·min^{-1}

Non-isothermal kinetics analysis In our current work, the Kissinger method[19] and the Ozawa-Doyle method[20] have been applied to evaluate the apparent activation energy (*E*) and the pre-exponential factor (*A*). The Kissinger Eqn. (1) and Ozawa Eqn. (2) are respectively given by

$$\ln\left(\frac{\beta}{T_p^{\,2}}\right) = \ln\frac{AR}{E} - \frac{E}{R}\frac{1}{T_p} \quad (1)$$

$$\log\beta + \frac{0.4567\ E}{RT_p} = C \quad (2)$$

where T_p is the peak temperature (°C); *A* is the pre-exponential factor (s^{-1}); *E* is the apparent activation energy (kJ mol^{-1}); *R* is the gas constant (8.314 J mol^{-1} K^{-1}); *β* is the linear heating rate (°C·min^{-1}) and *C* is a constant. According to the exothermic peak temperatures measured at the four different heating rates of 2, 5, 8, 10 °C min^{-1}, the thermokinetics parameters of the exothermal processes for the compound were determined by both the Kissinger and Ozawa-Doyle methods, including the apparent activation energies E_k, and E_o, pre-exponential factor A_k and linear correlation coefficients R_k and R_o, as listed in Table S7.

The calculated results extracted by the two both methods are quite close to each other and are all in the normal range of the kinetic parameters for the thermal decomposition reaction of solid materials.[21] The moderate E_a value (78.96 kJ mol^{-1}) for the thermal decomposition stage extrapolates that the exothermic process could not proceed spontaneously. Using the obtained E_a (the average of E_k and E_o) and ln *k* values, the Arrhenius equation for the exothermic process can be expressed as follows: ln $k = 6.407 - 78.96\times10^3/(RT)$, which can then be used to estimate the rate constant of the initial thermal decomposition process of the title compound.

Sensitivity The impact sensitivity (IF) was determined by using the falling hammer apparatus. A portion (20 mg) of the compound was compacted to a copper cap under the pressure of 39.2 MPa, and then was hit by a 2 kg drop hammer. The calculated value of *H*50 represents the drop height of the 50% initiation probability. The test result demonstrates that **1** does not ignite at the highest point of 200 cm (*H*50) corresponding to the impact energy of 40 J, indicating that **1** is insensitive to the impact. Under the same test condition, the impact sensitivities for TNT and RDX are 15 J, 7.5 J, respectively. Obviously, the impact sensitivity (IS) for the compound is lower than that of TNT. Friction sensitivity (FS) of the compound was measured by applying a Julius Peter's machine using 20 mg of the sample. No friction sensitivity (FS) was observed up to 36 kg (360 N). Additionally, the compound **1** was roughly tested for ESD (Electro-Static Discharge) sensitivity by spraying sparks across a small (5 crystals) sample of the material using a Tesla coil. Although unconfirmed by quantitative testing, the compound is most likely more insensitive to the electrostatic discharge than both TNT and RDX. The results advocate that the **1** is very insensitive to external stimuli ascribed to the structural characteristics of the compound, which probably arise from the fact that the N^{3-} anion could offer abundant coordination nodes bridging Co ions to generate compact 1D chain configuration.

Oxygen-bomb calorimetry To study the heat of combustion and enthalpy of formation of **1**, the constant-volume combustion energy (Δ_cU) was measured using a precise rotating-oxygen bomb calorimeter (RBC-II). To ensure safety and full combustion, prior to the measurement, 200 mg of the sample was pressed with 800 mg of benzoic acid to form a tablet. Recorded data were the average of six single measurements. The combustion of certified benzoic acid (Standard Reference Material, 39 j, NIST) in an oxygen atmosphere at the pressure of 30.5 bars was used to calibrate the calorimeter. The experimental result for the constant volume combustion energy of **1** was (–24590.02 ± 0.17) J·g^{-1}, which has an equivalence of (-18893.50 ± 0.9) kJ·mol^{-1} for the compound.

The standard molar enthalpy of combustion ($\Delta_cH_m^\theta$) of **1** is the combustion enthalpy change of the following ideal combustion reaction at 298.15 K and 101.325 kPa.

$Co_2C_{26}H_{30}N_{22}(s) + (69/2)O_2(g) =$

$$2CoO(s) + 26CO_2(g) + 15H_2O(l) + 11N_2(g) \quad (3)$$

The standard molar enthalpy of combustion of **1** was calculated according to:

$\Delta_cH_m^\theta = \Delta_cU + \Delta nRT$ and $\Delta n = n_g(\text{products}) - n_g(\text{reactants})$ (4)

where n_g represents the total molar amount of the gases present as products or reactants, with $R = 8.314$ J·mol^{-1}·K^{-1} and $T = 298.15$ K. The $\Delta_cH_m^\theta$ value could be derived as –18887.30 ± 0.9 kJ·mol^{-1}, equivalent to -24.58 MJ·kg^{-1}. As reported in the literature,[22] the enthalpies of combustion of RDX, HMX and TNT are 9.60 MJ·kg^{-1}, 9.44 to 9.88 MJ·kg^{-1} and 15.22 MJ·kg^{-1}, respectively. Accordingly, the enthalpy of combustion of the title compound is higher than those of RDX, HMX and TNT.

View Article Online
DOI: 10.1039/C8DT02335B

The standard molar enthalpy of formation of **1**, $\Delta_f H_m^\theta$, was calculated by Hess's law according to the following equation:

$\Delta_f H_m^\theta$ ($Co_2C_{26}H_{30}N_{22}$, s) = [2 $\Delta_f H_m^\theta$ (CoO, s) + 26 $\Delta_f H_m^\theta$ (CO_2, g) + 15 $\Delta_f H_m^\theta$ (H_2O, l)] – $\Delta_c H_m^\theta$ ($Co_2C_{26}H_{30}N_{22}$, s) (5)

where $\Delta_f H_m^\theta$ (CoO, s) = –237.94 kJ·mol^{-1}, $\Delta_f H_m^\theta$ (CO_2, g) = –393.51±0.13 kJ·mol^{-1} and $\Delta_f H_m^\theta$ (H_2O, l) = –285.83 ± 0.04 kJ·mol^{-1} were obtained from literature.[23] According to Hess's law, the standard molar enthalpy of formation for compound **1** at 298.15 K is calculated as being 3892.71 ± 0.17 kJ·mol^{-1}. Obviously, compared to the traditional energetic materials and some energetic metal coordination compounds, **1** provides a higher standard molar enthalpy of formation, producing considerable energy from the explosion, and making **1** a potential energetic CP.

Detonation properties Based on the largest exothermic principle proposed by Kamlet-Jacobs[24], a new empirical method reported by Pang et al.[25] was used to investigate the detonation properties of the metal-containing explosives without the use of sophisticated computer programs. The efficient method employed the hypothesis of the BKW equation and the arbitrary theory of the Kamlet-Jacobs method could be applied to evaluate the detonation properties of **1**. The detonation reaction estimated by the Pang's method was described by equation (6). The Kamlet-Jacobs equations were shown in equations (7)–(10).

$Co_2C_{26}H_{30}N_{22} \rightarrow 2\ Co(s) + 26\ C(s) + 10\ NH_3(g) + 6\ N_2(g)$ (6)

$D = 1.01\Phi^{1/2}(1+1.30\rho)$ (7)

$P = 1.558\rho^2\Phi$ (8)

$\Phi = 31.68N(MQ)^{1/2}$ (9)

$$Q = \frac{-\left[\Delta H_f(\text{detonation products}) - \Delta H_f(\text{energetic complex})\right]}{\text{formula weight of energetic complex}} \quad (10)$$

where D is the detonation velocity (km·s^{-1}), P is the detonation pressure (GPa), Q is the heat of detonation (kcal·g^{-1}), N is the number of moles of detonation gases per gram of explosive, M is the average molecular weight of the gases, and ρ is the density of the explosive (g·cm^{-3}). According to above equations, the heat of detonation (Q), detonation velocity (D) and detonation pressure (P) of **1** are calculated as 1.225 kcal·g^{-1}, 5.34 km·s^{-1} and 10.95 GPa, respectively.

For a comparison of the previously reported energetic materials and compound **1**, detailed thermochemical parameters are displayed in Fig.11 and Table 1. On account of a relatively high nitrogen content (N% = 40.10%), the heat of detonation (Q) of **1** is slightly higher than that of the partial traditional explosives [TNT (N% = 18.50%), CHHP (N% = 23.58%)] and is comparable to that of the previously reported energetic MOFs with similar nitrogen content, such as $\{[Cu(tztr)]\cdot H_2O\}_n$ (N% = 45.23%), $[Ag(atrz)_{1.5}(NO_3)]_n$ (N% = 43.76%). It is further emphasized that the high nitrogen content is the crucial factor for the assembly of high-energy materials with nitrogen-rich ligands. We note that the values of the detonation velocity (D) and detonation pressure (P) for **1** are smaller than those of the reported energetic materials derived from the inferior density of **1**. This indicates that a high density is conducive to the enhancement of the D and P. In addition, compound **1** is equipped with prominent insensitiveness (IS > 40 J and FS > 360N) based on its compact intrachain configuration. Furthermore, the decomposition products (cobalt**,** carbon, nitrogen and ammonia) of **1** are regarded as environmentally friendly. Therefore, **1** is considered to be an outstanding candidate environmentally friendly high-energy material by reason of its combination of favourable detonation performance and excellent safety.

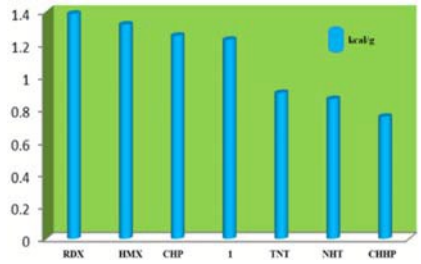

Fig. 11 Bar chart representation of the previously reported ΔH_{det} values for the common explosive materials, including TNT, RDX, HMX, CHP, NHT, CHHP. The ΔH_{det} value for **1** is also shown.

Table 1 Physicochemical properties of 1 and some representative energetic materials

	ρ [a] (g/cm^3)	N [b] (%)	T_{dec} [c] (ºC)	ΔH_{det} [d] (kcal/g)	D [e] (km/s)	P [f] (Gpa)	IS [g] (J)	FS [h] (N)
1	1.447	40.10	190	1.225	5.34	10.95	>40	>360
TNT[26]	1.654	18.50	244	0.897	7.178	20.50	15	353
RDX[26]	1.806	37.80	210	1.386	8.600	33.92	7.5	120
HMX[26]	1.950	37.80	280	1.320	8.900	38.39	7.4	-
CHP[27a]	1.948	14.71	194	1.250	8.225	31.73	0.5	-
NHP[27a]	1.983	33.49	220	1.370	9.184	39.69	-	-
CHHP[27b]	2.000	23.58	231	0.750	6.205	17.96	0.8	-
NHN[28]	2.156	40.14	-	0.859	7.3	20.2	-	-
$[Ag(atrz)_{1.5}(NO_3)]_n$[29a]	2.16	43.76	257	1.381	7.773	29.70	30	-
$\{[Cu(tztr)]\cdot H_2O\}_n$[29b]	2.316	45.23	80/325	1.322	7.92	31.99	>40	>360

[a] Density from X-ray diffraction. [b] Nitrogen content. [c] Thermal decomposition temperature. [d] Heat of detonation. [e] Detonation velocity. [f] Detonation pressure. [g] Impact sensitivity. [h] Friction sensitivity. CHP = Cobalt hydrazine perchlorate; NHP = Nickel hydrazine perchlorate; CHHP = Cobalt hydrazine hydrazinecarboxylate perchlorate, NHN = $[Ni(N_2H_4)_3(NO_3)_2]$.

Effects on thermal decomposition of AP and RDX To examine the effects of the thermal decomposition behaviors of AP and RDX after the addition of **1**, **1** was mixed with AP or RDX at the mass ratio of 1:3 (25%) to prepare the target samples. This study used DSC measurements with the heating rate of 10 ºC·min^{-1} in nitrogen atmosphere with Al_2O_3 as reference. A total sample mass of 0.8 mg was used for all runs. The DSC curves of pure AP and the mixtures of AP and title compound can be seen in Fig. 12a, and it can be seen that the endothermic peak of AP at 245 ºC arises from the crystal transformation of AP from the orthorhombic to the cubic phase.[30] The exothermic peak at 335 ºC is attributed to the partial decomposition of AP to form some intermediate products and then complete the decomposition to volatile

View Article Online
DOI: 10.1039/C8DT02335B

products.[31] There is no impact on the endothermic peak temperature of mixture sample, indicating that the crystal transition process of AP is hardly affected by **1**. It should be noted that the peak temperature (302 ºC) of the exothermic process is much lower than the exothermic peak temperature of AP (335 ºC). The above result illuminates that decomposition of AP is significantly accelerated by compound **1**. Furthermore, the curves for pure RDX and the mixture of RDX with compound **1** are shown in Fig. 12b, and it can be seen that the exothermic peak temperature of **1** (212 ºC) is lower than that of the pure RDX (246 ºC), supporting that the RDX decomposition is clearly promoted by compound **1**.

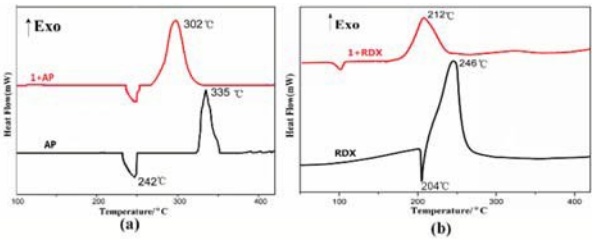

Fig. 12 (a) DSC curves of AP, **1**+AP and (b) DSC curves of RDX, **1**+RDX

Morphological Characterization To investigate the surface morphology of **1** and the solid products after the combustion of the mixture of **1** and AP (the residue remaining after the DSC measurement described above), the samples were characterized by SEM at low and high magnifications (Fig. 13). The crystals of the original compound **1** sample are regular strips with rough levelling off (Figs. 13a-b), which is ascribed to the uneven crystallization during the hydrothermal reaction. As seen from Figs. 13c-d, after the combustion of the mixture, the particles become small spheres. The large change in morphology is the result of the release of a large amount of gas during the combustion. This phenomenon indicates that the mixture has been fully burned.

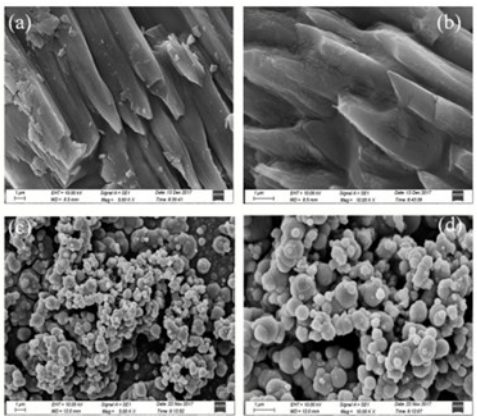

Fig. 13 SEM images of **1** (a,b), the residue after combustion from the mixture of AP and **1** (c,d)

Experimental

Physical Measurements

Elemental analysis (C, H, N) was administered with a Perkin-Elmer 2400 CHN elemental analyzer. The FT-IR spectra were conducted in the range 400-4000 cm^{-1} using KBr pellets on an EQUINOX55 FT/IR spectrophotometer. Thermogravimetric analysis (TGA) and differential scanning calorimetry (DSC) were performed on a CDR-4P thermal analyzer of Shanghai Balance Instrument factory and a Netzsch STA 449C instrument, respectively, using dry oxygen-free nitrogen as the atmosphere with a flowing rate of 10 $mL{\cdot}min^{-1}$. About 0.7 mg sample was sealed in aluminum pans in the temperature range of 30-500 °C for DSC experiments. The sensitivities to impact stimuli were determined by fall hammer apparatus applying standard staircase method using a 2 kg drop weight and the results were reported in terms of height for 50% probability of explosion ($h_{50\%}$).[32] The friction sensitivities were determined on a Julius Peter's apparatus by following the BAM method.[33]The constant-volume combustion energies of the compound was determined with a precise rotating-oxygen bomb calorimeter (RBC-type II).[34] The phase purity of the bulk or polycrystalline samples were recorded by powder X-ray diffraction (PXRD) measurements performed on a Rigaku RU200 diffractometer at 60 kV, 300 mA and Cu Kα radiation (λ = 1.5406 Å), with a scan speed of 5° min^{-1} and a step size of 0.02° in 2ϑ. Magnetic measurements were performed in the temperature range 2 K-300 K with an applied field of 1000 Oe, using a Quantum Design MPMS-XL-7 SQUID magnetometer on polycrystalline samples. Alternating current (ac) susceptibility experiments were performed using an oscillating ac field of 2.0 Oe at ac frequencies ranging from 1 to 1000 Hz.

Materials and methods

All of the solvents and reagents for synthesis are of analytical grade and are commercially available.

Caution! Although we have not encountered any problems in our experiments, azido and its complexes are potentially explosive; only a small amount of the materials should be prepared and disposed with care.

Synthesis

Preparation of $[Co_2(1\text{-mbt})_2(N_3)_4]_n$ (1)

The reactants $CoCl_2{\cdot}6H_2O$ (0.1 mmol, 0.024 g), NaN_3 (0.2 mmol, 0.013 g) and 1-mbt (0.1 mmol, 0.030 g) in ethanol solution (6 mL) were sealed in a 15 mL Teflon-lined stainless steel autoclave, heated at 140 °C, kept for 3 days, and then cooled to room temperature over 1 day. Blue crystals of **1** were obtained. (yield: 65%, based on Co). Anal. calcd for $C_{26}H_{30}Co_2N_{22}$ (768.54): C, 40.63; H, 3.93; N, 40.10%. Found: C, 40.61; H, 3.41; N, 40.12%. Main IR (KBr, cm^{-1}): 2077(s), 2056(s), 1476(m), 1161(m), 771(w), 750(w).

Crystallographic data collection and refinement

Suitable single crystal of the compound was mounted on glass fibers for X-ray measurements. Reflection data were collected at room temperature on a Bruker SMART APEX-CCD-based diffractometer using graphite mono-chromated Mo Kα radiation (λ = 0.71073 Å). An empirical absorption correction was applied using the SADABS program.[35] Data processing was

View Article Online
DOI: 10.1039/C8DT02335B

accomplished with the SAINT processing program. The structure was solved by the direct methods and refined with full-matrix least-squares on F^2 using SHELXH program.[36] All non-hydrogen atoms were refined with anisotropic displacement parameters. Selected crystallographic data and structural refinement details for **1** are summarized in Table 2. Selected bond lengths and bond angles of compound **1** are listed in Table S8.

Table 2 Selected crystallographic data and structural refinement for compound 1

	1
Empirical formula	$C_{26}H_{30}Co_2N_{22}$
Formula weight	768.54
Crystal system	triclinic
Space group	*P*-1
Temperature	293
a (Å)	11.2785(8)
b (Å)	12.5927(7)
c (Å)	12.8176(6)
α (°)	78.651(4)
β (°)	76.368(5)
γ (°)	75.469(5)
V (Å³)	1694.13(17)
Z	2
D (g/cm³)	1.447
μ (mm⁻¹)	8.139
F(0 0 0)	728.0
Unique reflections	6372
Observed reflections	12613
R_{int}	0.0228
Data/restraints/parameters	6372 /0 / 454
Final *R* indices	R_1 = 0.0443
R indices (all data)	R_1 = 0.0636
Goodness-of-fit on F^2	1.066

Computational methodology

The following computational methodology was used to calculate the coupling constant in the title compound.[37] The spin Hamiltonian proffered originally by Heisenberg can be written as $\hat{H} = -\sum_{(i>j)} JS_iS_j$ (where S_i and S_j are the spin operators of the paramagnetic centers, $S_i = S_j = 3/2$ for Co(II) ion; and the *J* constant is the coupling constant between the paramagnetic spin carriers), which can be employed to express the exchange coupling between two transition metal ions, the full Hamiltonian matrix for the entire system can be established. The *J* value was calculated from the energy difference of the two spin states: the broken symmetry (BS) state and the triplet state (HS), the broken symmetry approach along with electron correlations has been widely used to investigate magnetic properties in a large number of magnetic systems.[38] For comparison, the *J* values were extracted using three different equations that had been performed on cobalt(II)-containing systems reported previously,[39] as follows:

$$J = -\frac{E_{HS} - E_{BS}}{S_{max}^2} \quad (11)$$

$$J = -\frac{E_{HS} - E_{BS}}{S_{max}(S_{max} + \mathbf{1})} \quad (12)$$

$$J = -\frac{E_{HS} - E_{BS}}{S_{HS}^2 - S_{BS}^2} \quad (13)$$

where E_{BS} is the energy of the broken symmetry state and E_{HS} is the energy of the triplet state.

The DFT calculations are implemented with the ORCA 3.0.2 package.[40] The BP86 functional proposed by Becke[41] and Perdew[42] and hybrid B3LYP functional built by Becke[41] and Perdew *et al*[42] were applied in the calculation, respectively. The double-ξ quality plus polarization def2-SVP basis set and polarized triple-quality basis sets of def2-TZVP, TZVP, and TZV proposed by Ahlrichs and co-workers were respectively performed for all atoms.[43] The calculation model for the compound was built from the experimental results.

To obtain the single-ion magnetic property of **1**, *ab initio* calculations have been performed with ORCA software. Post-Hartree–Fock CASSCF calculations were carried out to evaluate the potential magnetic anisotropies of Co(II) ions. The computation program was utilized to complete CASSCF/NEVPT2 calculations[44–46] for CASSCF(7,5) using the scalar relativistic contracted version of def2-TZVP basis functions.[47]

Conclusions

In summary, a 1D azido-Co(II) compound, $[Co_2(1\text{-mbt})_2(N_3)_4]_n$, in which azido spacers adopt novel coordination pattern of alternating [-EE-EO-EO-EO-]$_n$, was synthesized and continuously investigated in order to develop its multifunctionality in the fields of molecular magnets and high-energy materials. Magnetic investigation unveils that the coexistence of F and AF coupling between the Co(II) ions within the metal chains is caused by the mixed EO-azido and EE-azido bridges, respectively. Compound **1** behaves as field-induced slow magnetic relaxation with the effective energy barrier of U_{eff} = 22.46 K owing to the synergistic effect of single-ion magnetic anisotropy and intermetallic magnetic coupling. The exploration of the energetic performance verifies that compound **1** displays potential application as a new generation of environmentally friendly high-energy materials derived from its high nitrogen content (N = 40.10%) and oxygen-free system. The heat of detonation of **1** is higher than that of the traditional energetic materials (TNT, CHHP), and is comparable the values for some reported energetic MOFs, such as $\{[Cu(tztr)]\cdot H_2O\}_n$, $[Ag(atrz)_{1.5}(NO_3)]_n$. DSC experiments expose that the compound can effectively accelerate the decompositions of AP and RDX. Meanwhile, compound **1** exhibits favourable safety and insensitiveness characteristics relied on its compact intrachain configuration. The present work exploits the probable application of **1** in the field of advanced magneto-energetic materials, and additional results are expected with the further development of relevant work.

View Article Online
DOI: 10.1039/C8DT02335B

Acknowledgements

We gratefully acknowledge the financial support from the National Natural Science Foundation of China (21463020, 21766026 and 21673180), the Foundation for Fostering Outstanding Young Teachers of Ningxia Higher Education Institutions of China (NGY2016063), the Graduate Innovative Experiment (GIP2018040), the National Undergraduate Innovative and Entrepreneurial Training Program (201810749009), and the Foundation of State Key Laboratory of High-efficiency Utilization of Coal and Green Chemical Engineering (2016-14).

References

1 (a) L. E. Kreno, K. Leong, O. K. Farha, M. Allendorf, R. P. Van Duyne and J. T. Hupp, *Chem. Rev.*, 2012, **112**, 1105-1125; (b) D. Liu, K. Lu, C. Poon and W. Lin, *Inorg. Chem.*, 2014, **53**, 1916-1924. (c) J. Y. Liang, G. P. Li, R. C. Gao, N. N. Bai, W. Q. Tong, L. Hou and Y. Y. Wang, *Crystal Growth & Design*, 2017, **17**, 6733-6740.

2 (a) R. B. Getman, Y. S. Bae, C. E. Wilmer and R. Q. Snurr, *Chem. Rev.*, 2012, **112**, 703-723; (b) D. Alezi, Y. Belmabkhout, M. Suyetin, P. M. Bhatt, Ł. J. Weseliński, V. Solovyeva and M. Eddaoudi, *J. Am. Chem. Soc.*, 2015, **137**, 13308-13318; (c) J. Jiang, H. Furukawa, Y. B. Zhang and O. M. Yaghi, *J. Am. Chem. Soc.*, 2016,**138**, 10244-10251.

3 (a) A. Y. Robin and K. M. Fromm, *Coord. Chem. Rev.*, 2006, **250**, 2127-2157; (b) W. Lee Leong and J. J. Vittal, *Chem. Rev.*, 2010, **111**, 688-764; (c) Y. Q. Wang, Q. Yue and E. Q.Gao, *Chem. Eur. J.*, 2017, ***23***, 896-904; (d) X. Y. Liu, X. H. Ma, P. P. Cen, Y. W. Wu, C. C. Zhang, Q. Shi, W. M. Song, G. Xie, and S. P. Chen, *Dalton Trans.*, 2017, **46**, 7556-7566.

4 (a) D. Skinner, D. Olson and A. Block-Bolten, *Propellants, Explos., Pyrotech.*, 1998, **23**, 34-42; (b) S. Zhang, Q. Yang, X. Y. Liu, X. N. Qu, Q. Wei, G. Xie, S. P. Chen and S. L. Gao, *Coord. Chem. Rev.,* 2016, **307**, 292-312; (c) Q. Yang, G. L.Yang, W. D. Zhang, S. Zhang, Z. H. Yang, G. Xie, S. P. Chen and S. L. Gao, *Chem. Eur. J.*, 2017, **23**, 9149-9155.

5 (a) V. E. Campbell, R. Guillot, E. Riviere, P. T. Brun, W. Wernsdorfer and T. Mallah, *Inorg. Chem.*, 2013, **52**, 5194-5200; (b) Y. Z. Zheng, Z. Zheng and X. M. Chen, *Coord. Chem. Rev.*, 2014, **258**, 1-15; (c) R. Modak, Y. Sikdar, G. Cosquer, S. Chatterjee, M. Yamashita and S. Goswami, *Inorg. Chem.*, 2015, **55**, 691-699; (d) Y. S. Meng, S. D. Jiang, B. W. Wang and S. Gao, *Accounts chem. Res.*, 2016, **49**, 2381-2389.

6 M. Mannini, F. Pineider, P. Sainctavit, C. Danieli, E. Otero, C. Sciancalepore, A. M. Talarico, M. A. Arrio, A. Cornia, D. Gatteschi and R. Sessoli, *Nat. Mater.*, 2009, **8**, 194–197.

7 R. E. Winpenny, *Angew. Chem., Int. Ed.*, 2008, **47**, 7992–7994.

8 L. Bogani and W. Wernsdorfer, *Nat. Mater.*, 2008, **7**, 179–186.

9 (a) M. Murrie, *Chem. Soc. Rev.*, 2010, **39**, 1986-1995; (b) X. Y. Liu, L. Sun, H. L. Zhou, P. P. Cen, X. Y. Jin, G. Xie, S. P. Chen and Q. L. Hu, *Inorg. Chem.,* 2015, **54**, 8884-8886; (c) X. Y. Liu, X. N. Qu, S. Zhang, H. S. Ke, Q. Yang, Q. Shi, G. Xie, S. P. Chen, *Inorg. Chem.,* 2015, **54**, 11520-11525; (d) X. Y. Hou, X. Wang, X. Y. Liu, J. J. Wang, L. Tang, P. Ju, *New J. Chem.*, 2018, **42**, 8583-8590; (e) L. Chen, S. Y. Chen, Y. C. Sun, Y. M. Guo, L. Yu, X. T. Chen, Z. X. Wang, T. H. Ouyang, Y. Song, Z. L. Xue, *Dalton Trans.*, 2015, **44**, 11482-11490.

10 (a) Y. F. Zeng, X. Hu, F. C. Liu and X. H. Bu, *Chem. Soc. Rev.*, 2009, **38**, 469-480; (b) J. P. Zhao, R. Zhao, W. C. Song, Q. Yang, F. C. Liu and X. H. Bu, *Cryst. Growth. Des.*, 2013, **13**, 437-439; (c) X. Y. Liu, F. F. Li, X. H. Ma, P. P. Cen, S. C. Luo, Q. Shi, S. R. Ma, Y. W. Wu, C. C. Zhang, Z. Xu, W. M. Song, G. Xie, S. P. Chen, *Dalton Trans.*, 2017, **46**, 1207-1217; (d) J. P. Zhao, C. Zhao, W. C. Song, L. Wang, Y. Xie, J. R. Li and X. H. Bu, *Dalton Trans.*, 2015, **44**, 10289-10296; (e) X. T. Wang, Z. M. Wang and S. Gao, *Inorg. Chem.*, 2007, **46**, 10452-10454; (f) Y. Ma, J. Y. Zhang, A. L. Cheng, Q. Sun and E. Q. Gao, C. M. Liu, *Inorg. Chem.*, 2009, **48**, 6142-6151; (g) X. T. Wang, X. H. Wang, Z. M. Wang and S. Gao, *Inorg. Chem.*, 2009, **48**, 1301-1308.

11 (a) K. S. Lim, D. W. Ryu, W. R. Lee, E. K. Koh, H. C. Kim and C. S. Hong, *Chem.–Eur. J.*, 2012, **18**, 11541–11544; (b) S. Mukherjee and P. S. Mukherhee, *Acc. Chem. Res.*, 2013, **46**, 2556–2566; (c) J. P. Zhao, Y. Xie, J. R. Li and X. H. Bu, *Dalton Trans.*, 2016, **45**, 1514-1524; (d) S. Ghosh, S. Roy, C. M. Liu and S. Mohanta, *Dalton Trans.*, 2018, **47**, 836–844.

12 (a) H. B. Xu, B. W. Wang, F. Pan, Z. M. Wang and S. Gao, *Angew. Chem., Int. Ed.*, 2007, **46**, 788–7392; (b) D. F. Weng, Z. M. Wang and S. Gao, *Chem. Soc. Rev.*, 2011, **40**, 3157–3181; (c) Z. X. Li, Y. F. Zeng, H. Ma and X. H. Bu, *Chem. Commun.*, 2010, **46**, 8540–8542.; (d) X. H. Zhao, L. D. Deng, Y. Zhou, D. Shao, D. Q. Wu, X. Q. Wei and X. Y. Wang, *Inorg. Chem.*, 2017, **56**, 8058-8067.

13 (a) M. Talawar, R. Sivabalan, T. Mukundan, H. Muthurajan, A. Sikder, B. Gandhe and A. S. Rao, *J. Hazard. Mater.*, 2009, **161**, 589–607; (b) Y. C. Li, C. Qi, S. H. Li, H. J. Zhang, C. H. Sun, Y. Z. Yu and S. P. Pang, *J. Am. Chem. Soc.*, 2010, **132**, 12172–12173.

14 H. Zhao, Z. R. Qu, H. Y. Ye and R. G. Xiong, *Chem. Soc. Rev.*, 2008, **37**, 84–100.

15 E. Ramos, J. E. Román, S. Cardona-Serra and J. M. Clemente-Juan, *Comput. Phys. Commun.*, 2010, **181**, 1929-1940.

16 (a) J. Ribas, A. Escuer, M. Monfort, R. Vicente, R. Corte´ s, L. Lezama and T. Rojo, *Coord. Chem. Rev.*, 1999, **1027**, 193–195; (b) A. Escuer and G. Aromı´, *Eur. J. Inorg. Chem.*, 2006, **23**, 4721-4736; (c) X. Y. Wang, Z. M. Wang and S. Gao, *Chem. Commun.*, 2008, **3**, 281-294.

17 (a) K. Bernot, L. Bogani, A. Caneschi, D. Gatteschi and R. Sessoli, *J. Am. Chem. Soc.*, 2006, **128**, 7947-7956; (b) R. J. Glauber, *J. Math. Phys.*, 1963, **4**, 294-307; (c) A. Saitoh, H. Miyasaka, M. Yamashita and R. Clerac, *J. Mater. Chem.*, 2007, **17**, 2002-2012.

18 J. Cano, Y. Journaux, M. S. A. Goher, M. A. M. Abu-Youssef, F. A. Mautner, G. J. Reiâ, A. Escuer and R. Vicente, *New J. Chem.*, 2005, **29**, 306.

19 H. E. Kissinger, *Anal. Chem.*, 1957, **29**, 1702–1706.

20 (a) T. Ozawa, *Bull. Chem. Soc. Jpn.*, 1965, **38**, 1881–1886; (b) C. D. Doyle, *J. Appl. Polym. Sci.*, 1961, **5**, 285–292.

21 R. Z. Hu, Z. Q. Yang and Y. J. Liang, *Thermochim. Acta.*, 1988, **123**, 135–151.

22 Y. X. Ou, Explosives, Beijing Institute of Technology Press, China, 2006.

23 J. D. Cox, D. D. Wagman and V. A. Medvedev, CODATA Key Values for Thermodynamics. Hemisphere Publishing Corp., New York, **1989**.

24 M. J. Kamlet and S. Jacobs, *J. Chem. Phys.*, 2003, **48**, 23–35.

25 Y. Wang, J. C. Zhang, H. Su, S. H. Li, S. W. Zhang and S. P. Pang, *J. Phys. Chem. A*, 2014, **118**, 4575–4581.

26 J. Köhler and R. Meyer, Explosivstoffe, 9th edn, Wiley-VCH, Weinheim, **1998**.

27 (a) O. S. Bushuyev, P. Brown, A. Maiti, R. H. Gee, G. R. Peterson, B. L. Weeks and L. J. Hope-Weeks, *J. Am. Chem. Soc.,* 2012, **134,** 1422–1425; (b) O. S. Bushuyev, G. R. Peterson, P. Brown, A. Maiti, R. H. Gee, B. L. Weeks and L. J. Hope-Weeks, *Chem. Eur. J.,* 2013, **19**, 1706–1711.

28 O. S. Bushuyev, P. Brown, A. Maiti, R. H. Gee, G. R. Peterson, B. L. Weeks and L. J. Hope-Weeks, *J. Am. Chem. Soc.*, 2012, **134**, 1422-1425.

29 (a) S. H. Li, Y. Wang, C. Qi, X. X. Zhao, J. C. Zhang, S. W. Zhang and S. P. Pang, *Angew. Chem.,* 2013, **52,** 14031–14035; (b) X.

View Article Online
DOI: 10.1039/C8DT02335B

Y. Liu, W. J. Gao, P. P. Sun, Z. Y. Su, S. P. Chen, Q. Wei, G. Xie and S. L. Gao, *Green Chem.*, 2015, **17**, 831-836.
30 J. A. Creighton and D. G. Eadon, *J. Chem. Soc. Faraday Trans.*, 1991, **87**, 3881-3891.
31 (a) W. A. Rosser and S. H. Inami, *Combust. Flame*, 1968, **12,** 427-435; (b) P. W. M. Jacobsete and G. S. Pearson, *Combust. Flame*, 1969, **13**, 419-430.
32 R. Meyer and J. Köhler (Eds.), *Explosives*, 4th ed. revised and extended, VCH Publishers, New York, 1993, 149-150.
33 R. Meyer and J. Köhler (Eds.), *Explosive*s, 4th ed. revised and extended, VCH Publishers, New York, 1993, 197-199.
34 X. Yang, S. Chen, S. Gao, H. Li and Q. Shi, *Instrum Sci. Technol.*, 2002, **30**, 311-321.
35 G. M. Sheldrick, SADABS, Program for Empirical Absorption Correction for Area Detector Data, University of Go ¨ttingen, Go ¨ttingen, Germany, 1996.
36 G. M. Sheldrick, SHELXS-2014 and SHELXL-2014, Program for Crystal Structure Determination, University of Go ¨ttingen, Go ¨ttingen, Germany, 2014.
37 (a) E. Ruiz, P. Alemany, S. Alvarez and J. Cano, *J. Am. Chem. Soc.*, 1997, **119**, 1297–1303; (b) E. Ruiz, A. Rodrı´guez-Fortea, J. Cano, S. Alvarez and P. Alemany, *J. Comput. Chem.*, 2003, **24**, 982–989; (c) E. Ruiz, J. Cano, S. Alvarez and P. Alemany, *J. Comput. Chem.*, 1999, **20**, 1391–1400; (d) E. Ruiz, *Struct. Bonding*, 2004, **113**, 71–102.
38 (a) S. Sarkar, A. Datta, A. Mondal, D. Chopra, J. Ribas, K. K. Rajak, S. M. Sairam and S. K. Pati, *J. Phys. Chem. B*, 2006, **110**, 12–15; (b) E. Cremades and E. Ruiz, *Inorg. Chem.*, 2010, **49**, 9641–9648; (c) B. Gole, R. Chakrabarty, S. Mukherjee, Y. Song and P. S. Mukherjee, *Dalton Trans.*, 2010, **39**, 9766–9778.
39 (a) J. D. Leng, S. K. Xing, R. Herchel, J. L. Liu and M. L. Tong, *Inorg. Chem.*, 2014, **53**, 5458-5466; (b) A. V. Funes, L. Carrella, L. Sorace, E. Rentschler and P. Alborés, *Dalton Trans.*, 2015, **44**, 2390-2400; (c) S. S. Massoud, M. Spell, C. C. Ledet, T. Junk, R. Herchel, R. C. Fischer, Z. Trávníček and F. A. Mautner, *Dalton Trans.,* 2015, **44**, 2110-2121; (d) M. Rams, Z. Tomkowicz, M. Böhme, W. Plass, S. Suckert, J. Werner, I. Jess and C. Näther, *Phys. Chem. Chem. Phys.,* 2017, **19**, 3232-3243.
40 (a) F. Neese, ORCA-an ab initio, Density Functional and Semiempirical Program Package, 3.0.1, University of Bonn, Bonn, Germany, 2013, http://www.thch.uni-bonn.de/tc/orca/; (b) F. Neese, *Wiley Interdiscip. Rev.: Comput. Mol. Sci.*, 2012, **2**, 73–78.
41 A. D. Becke, *Phys. Rev. A*, 1988, **38**, 3098–3100.
42 J. P. Perdew, *Phys. Rev. B*: *Condens. Matter Mater. Phys.*, 1986, **33**, 8822–8824.
43 A. Scha ¨fer, H. Horn and R. Ahlrichs, *J. Chem. Phys.*, 1992, **97**, 2571-2577.
44 P. A. Malmqvist and B. O. Roos, *Chem. Phys. Lett.*, 1989, 155, 189–194.
45 C. Angeli, R. Cimiraglia and J.-P. Malrieu, *J. Chem. Phys.*, 2002, 117, 9138–9153.
46 C. Angeli, S. Borini, M. Cestari and R. Cimiraglia, *J. Chem. Phys.*, 2004, 121, 4043–4049.
47 D. A. Pantazis, X.-Y. Chen, C. R. Landis and F. J. Neese, *J. Chem. Theory Comput.*, 2008, 4, 908–919.